Journal of Solid State Chemistry **157,** 225–232 (2001)
doi:10.1006/jssc.2000.9080, available online at http://www.idealibrary.com on IDEAL®

Structure and Physical Properties of the New Pseudo-binary Intermetallic Compound $Ti_{11}(Sb, Sn)_8$

Hyungrak Kim,* Marilyn M. Olmstead,* Julia Y. Chan,† Paul C. Canfield,‡ Ian R. Fisher,‡ Robert W. Henning,§ Arthur J. Schultz,§ and Susan M. Kauzlarich*,[1]

*Department of Chemistry, University of California—Davis, One Shields Avenue, Davis, California 95616; †Department of Chemistry, Louisiana State University, Baton Rouge, Louisiana 70803; ‡Department of Physics, Iowa State University, Ames, Iowa 50011; and §IPNS Division, Argonne National Laboratory, Argonne, Ilinois 60439

Received September 19, 2000; in revised form December 4, 2000

The new pseudo-binary intermetallic compound, $Ti_{11}(Sb, Sn)_8$, has been synthesized by reacting Ti and Sb in a Sn flux at 1100°C and its structure determined from both single-crystal X-ray and neutron diffraction data (orthorhombic, *Pnma*, Z = 4, X-ray diffraction at 90 K: $a = 14.6877(6)$ Å, $b = 5.5677(2)$ Å, $c = 17.7207(7)$ Å, $V = 1449.14(10)$ Å^3, neutron diffraction at room temperature: $a = 14.677(6)$ Å, $b = 5.577(3)$ Å, $c = 17.716(6)$ Å, $V = 1450(1)$ Å^3). The structure contains two differently oriented repeating layers and interstitial atoms that are closely connected to make linear chains aligned along the crystal *b* axis. The compound exhibits mixed site occupancies of Sb and Sn on the anion sites. The phase width (Sb/Sn ratio = 0.98–1.40) was determined by microprobe elemental analysis. The electrical resistivity of a single crystal as a function of temperature is anisotropic ($\rho_{//b} = 1 \sim 2 \times 10^{-1}$ mΩ·cm, $\rho_{\perp b} = 0.5 \times 10^{-1}$ mΩ·cm) and confirms that this compound is metallic. Magnetic susceptibility measurements show Pauli paramagnetism. © 2001 Academic Press

Key Words: **pseudo-binary titanium intermetallic; Sn flux; mixed occupancy; differential site occupancy; electrical anisotropy; Pauli paramagnetic.**

INTRODUCTION

The site preference of different elements for specific crystallographic positions has long been a focus in solid state chemistry because of its essential relationship with physical properties. Electronic structure calculations have provided insights to the understanding of the arrangement of elements in a given structure. In a recent review (1), site energy and bond energy based on valence electron concentration (*vec*) are regarded as the fundamental energetic contributions that influence how elements order in a structure. These two parts of the total electronic energy were examined to find the relationship among the observed structure, compositions, and properties of intermetallics and transition metal cluster compounds.

In the past decade, a new concept of site preferences, especially with regard to the early transition metal sulfides and phosphides, has been proposed by Franzen and Köckerling (2). This idea has been applied to ternary compounds of the type $M_xM'_yX$, where M and M' are two transition metals and X is an element of group 15 or 16. The structures are stabilized by differential fractional site occupancy (DFSO) of the metals from site to site. The preferences of the metal for specific sites are explained by the chemical bonding character represented by Mulliken overlap populations (MOP) (3). Using this approach, many unknown phases of pseudo-binary compounds have been synthesized (4–6).

In this article, a pseudo-binary phase of the transition metal (Ti) with the main group elements (Sn and Sb) is reported. The $Ti_{11}(Sb, Sn)_8$ compound is isostructural to the recently reported $Ti_{10.84}Sb_{7.73}$ (7) and $(Zr, V)_{11}Sb_8$ (8) compounds and to the transition metal germanides $Cr_{11}Ge_8$ (9) and $Mn_{11}Ge_8$ (10). In the $(Zr, V)_{11}Sb_8$ compound, mixed occupancies of Zr and V on two of the metal sites were reported, and the preferences were explained by the DFSO concept based on the differences in size, electronegativity, and valence-electron numbers of Zr and V. The title compound, however, shows mixed occupancies of main group elements in the anion sites. Site preferences of the Sb and Sn atoms and physical properties of the compound are discussed. Temperature-dependent resistivity and magnetism are presented.

EXPERIMENTAL SECTION

Synthesis. Crystals of $Ti_{11}(Sb, Sn)_8$ were unintentionally prepared while investigating the Sn-flux synthesis (11) of the

[1] To whom correspondence should be addressed. Fax: (530)752-8995. E-mail: smkauzlarich@ucdavis.edu.

0022-4596/01 $35.00

hypothetical rare earth transition metal compound (12), $Yb_{14}TiSb_{11}$. The synthesis of single crystals of $Ti_{11}(Sb, Sn)_8$ using Sn flux was successfully repeated by heating the mixture of Ti and Sb in a Sn flux (Ti:Sb:Sn mole ratio = 11:4.5:89) at 1100°C for 1 h with a cooling rate of 2°C/h to 700°C. Titanium (Johnson Matthey, 99.99%, $\approx$ 20 mesh), 1 $\sim$ 3 mm antimony shot (CERAC, 99.999%), and tin granules (Alfa, 99.99%) were used for the reaction.

The elements were placed into an alumina crucible capped with quartz wool and sealed in a quartz ampoule under $\frac{1}{5}$ atm pressure of purified Ar. The reactants were handled in a N_2-filled drybox with water levels less than 1 ppm. The quartz ampoule containing products was spun in a centrifuge to remove the Sn-flux liquid from crystals at the final temperature of 700°C. Highly reflective needle-shaped crystals grown from the wall of the alumina crucible in the flux reaction were used for X-ray structure determination and physical property measurements. These crystals are stable in air.

The same phase powder product was also made by reacting the stoichiometric amount of elements (Ti:Sb:Sn, 11:4.5:3.5) in a sealed tantalum tube at 1100°C for 10 days. Experimental X-ray diffraction patterns were compared with that calculated from single-crystal X-ray data for $Ti_{11}(Sb, Sn)_8$ by CrystalDiffract v 2.0 (13). In a similar fashion, attempts were made to synthesize the two end members of the title compound, $Ti_{11}Sb_8$ and $Ti_{11}Sn_8$. Synthesis of the As analog of the title compound, $Ti_{11}As_{4.5}Sn_{3.5}$, was also attempted by heating the stoichiometric elements (Ti:As:Sn, 11:4.5:89) in an alumina crucible using Sn-flux reaction and by heating the elements (Ti:As:Sn, 11:4.5:3.5) in a sealed tantalum tube at 1100°C for 10 days.

Structure determination. Single-crystal X-ray diffraction data of a crystal ($0.08 \times 0.09 \times 0.12$ mm^3) were collected using a Bruker SMART 1000 CCD diffractometer equipped with a CRYO COOLER low-temperature apparatus (CRYO INDUSTRIES of America, Inc.). X-rays were generated at 50 kV and 40 mÅ using a Mo target and graphite monochromator. Data collection parameters and crystallographic data are provided in Table 1. A total of 1421 frames were measured with a 0.3° ω rotation and 30-s acquisition time. The SMART software (14) was used for data collection and SAINT (15) for data integration. The absorption correction was performed using SADABS. The structure was solved by direct methods and refined using SHELXL-97 (16). Several models were investigated to determine the anion site occupancy of Sb and Sn. In all cases, the wR_2 was not improved significantly, indicating that it is impossible to distinguish Sb and Sn atoms by X-ray diffraction because of their similar scattering factors (17). Atomic coordinates and isotropic thermal parameters and important distances are listed in Table 3 and Table 4, respectively. X-ray powder diffraction data of the products were obtained using an Enraf-Nonius Guinier camera equipped with a quartz monochromator that gave Cu$K\alpha_1$ radiation. Powdered silicon (NBS) was included in the samples as an internal standard.

TABLE 1
Crystallographic Data of X-Ray Diffraction

Formular	$Ti_{11}(Sb, Sn)_8$
Temperature (K)	90
Radiation	Mo$K\alpha$, $\lambda = 0.71073$ Å
Space group	*Pnma*
Lattice parameters (Å)	$a = 14.6877(6)$
	$b = 5.5677(2)$
	$c = 17.7207(7)$
Cell Volume (Å^3)	$V = 1449.14(10)$
Z	4
Dimension (mm^3)	$0.08 \times 0.09 \times 0.12$
$\rho_{calc.}$ (g/cm^3)	6.897
μ Mo$K\alpha$ (mm^{-1})	20.27
θ range	$0° < \theta < 31.48°$
Scan range (ω) (°)	0.3
Number of collected reflections	2706
Number of unique reflections	2548
Number of parameters refined	106
R_1 for $F_o^2 > 2\sigma(F_c^2)$, (%)[a]	3.41
wR_2 (%)[b]	8.46
$(\Delta\rho)_{max}$, $(\Delta\rho)_{min}$ (e Å^{-3})	2.894, $-$ 3.432

[a] $R_1 = \sum ||F_o| - |F_c|| / \sum |F_o|$.
[b] w$R_2 = [\sum[w(F_o^2 - F_c^2)^2] / \sum[w(F_o^2)^2]]^{1/2}$, $w^{-1} = [\sigma^2(F_o^2) + (0.0305p)^2 + 28.39P]$, where $p = [\max(F_o^2, 0) + 2F_c^2]/3$.

Neutron data collection. A single crystal ($1 \times 1 \times 3$ mm^3) was mounted on an aluminum pin with epoxy and placed on the single-crystal diffractometer (SCD) at the intense pulsed neutron source (IPNS) at Argonne National Laboratory (18). One histogram of data was collected to check for crystal quality and to determine the initial orientation matrix using an auto-indexing routine (19). The lattice parameters for the $Ti_{11}(Sb, Sn)_8$ structure were easily obtained but a few weakly diffracting peaks could not be indexed (see Table 2). These extra peaks had d spacings corresponding to elemental tin and were believed to originate from small tin crystallites on the surface of the crystal. Sixteen time-of-flight histograms were collected with different χ and ϕ settings and covered approximately one octant of data (h, k, l). Bragg reflections in each histogram were integrated and corrected for the Lorentz factor and the incident spectrum (20). A wavelength-dependent spherical absorption correction was applied but symmetry-related reflections were not averaged because of the wavelength dependence of extinction.

The overall framework was already established with the X-ray data set so these positions were used as a starting point in the neutron refinement. The initial refinements were performed with only Ti and Sb in the structure and yielded

TABLE 2
Data Collection Parameters and Crystallographic Data of Neutron Diffraction

Temperature (°C)	23
Crystal size (mm^3)	$1 \times 1 \times 3$
Space group	*Pnma* (No. 62)
a (Å)	14.677(6)
b (Å)	5.577(3)
c (Å)	17.716(6)
V ($Å^3$)	1450(1)
Z	4
Radiation	Neutrons, $\lambda = 0.7$–4.2 Å
Data collection technique	TOF Laue with position-sensitive area detector
$\mu(\lambda)$ (cm^{-1})	$0.218 + 0.163 \cdot \lambda$
Extinction parameter (rad^{-1})	$4.2(2) \times 10^{-5}$
No. of refls in final ls with $F_o^2 > 3\sigma(F_o^2)$	1699
No. of unique reflections	1262
No. of variables	122
Function minimized	$\sum w(F_o - F_c)^2$
$R_w(F^2)^a$	0.101
$R(F^2)^b$	0.160
$R_w(F)^c$	0.051
$R(F)^d$	0.088
GOF	1.46

[a] $R_w(F^2) = [\sum[w(F_o^2 - F_c^2)^2]/\sum[w|F_o^2|]]^{1/2}$.
[b] $R(F^2) = \sum[|F_o^2 - F_c^2|]/\sum[|F_o^2|]$.
[c] $R_w(F) = [\sum[w(F_o - F_c)^2]/\sum[w|F_o|]]^{1/2}$.
[d] $R(F) = \sum[|F_o - F_c|]/\sum[|F_o|]$.

an $R(F)$ factor of 8.8% with both the atomic positions and anisotropic thermal parameters refining. The atomic positions agreed quite well with the X-ray data and all of the thermal parameters were positive, suggesting that tin was

TABLE 3
Atomic Coordinates and Equivalent Isotropic Displacement Parameters (X-Ray)

Atom	x	y	z	U(eq)
Sb(1)	0.29573(4)	¼	0.30280(3)	0.00160(11)
Sb(2)	0.44065(4)	¼	0.51750(3)	0.00211(11)
Sb(3)	0.08345(4)	¼	0.19517(3)	0.00175(11)
Sb(4)	0.22568(4)	¼	0.90783(3)	0.00243(12)
Sb(5)	0.01557(4)	¼	0.74313(3)	0.00253(12)
Sb(6)	0.04969(4)	¼	0.43717(4)	0.00921(14)
Sb(7)	0.28623(3)	0.0028(1)	0.10896(2)	0.00347(10)
Ti(1)	0.43368(11)	¼	0.19335(9)	0.00310(27)
Ti(2)	0.12557(10)	¼	0.04127(9)	0.00276(26)
Ti(3)	0.20080(11)	¼	0.74917(9)	0.00272(27)
Ti(4)	0.36661(10)	¼	0.66168(9)	0.00269(26)
Ti(5)	0.24934(11)	¼	0.46603(9)	0.00287(27)
Ti(6)	0.04287(12)	¼	0.59262(10)	0.00705(30)
Ti(7)	0.36595(11)	0.0112(2)	0.82516(6)	0.00228(19)
Ti(8)	0.38149(11)	¼	0.99134(10)	0.00718(30)
Ti(9)	0.06036(7)	0.0020(2)	0.87901(6)	0.00212(19)

TABLE 4
Coordination Environment of Each Site in $Ti_{11}(Sb, Sn)_8$

Sb(1)	Ti(1)	2.8048(17)	Ti(1)	Sb(1)	2.8048(17)
	Ti(7)	2.8127(12)		Sb(6)	2.8728(17)
	Ti(9)	2.8740(12)		Sb(3)	2.9567(17)
	Ti(3)	2.9420(6)		Sb(7)	2.9699(15)
	Ti(5)	2.9716(6)		Sb(5)	3.0139(7)
Sb(2)	Ti(4)	2.7766(17)	Ti(2)	Sb(4)	2.7845(17)
	Ti(9)	2.8270(12)		Sb(3)	2.7965(17)
	Ti(9′)	2.8915(12)		Sb(2)	2.9090(16)
	Ti(2)	2.9090(16)		Sb(2′)	2.9788(6)
	Ti(5)	2.9542(17)		Sb(7)	2.9834(14)
	Ti(2)	2.9788(6)	Ti(3)	Sb(5)	2.7226(17)
Sb(3)	Ti(2)	2.7965(17)		Sb(4)	2.8351(17)
	Ti(7)	2.8237(12)		Sb(7)	2.8622(14)
	Ti(9)	2.8563(12)		Ti(4)	2.8870(22)
	Ti(4)	2.9394(5)		Sb(1)	2.9420(6)
	Ti(1)	2.9567(17)	Ti(4)	Sb(5)	2.7628(16)
Sb(4)	Ti(8)	2.7253(17)		Sb(2)	2.7766(17)
	Ti(2)	2.7845(17)		Sb(7)	2.8096(14)
	Ti(3)	2.8351(17)		Ti(3)	2.8870(22)
	Ti(9)	2.8395(12)		Sb(3)	2.9394(5)
	Ti(7)	2.8563(12)	Ti(5)	Sb(7)	2.9445(14)
	Ti(5)	2.9913(6)		Sb(2)	2.9542(17)
Sb(5)	Ti(6)	2.6971(18)		Sb(1)	2.9716(17)
	Ti(3)	2.7226(17)		Sb(6)	2.9767(17)
	Ti(4)	2.7628(16)		Sb(4)	2.9913(6)
	Ti(7)	2.8394(12)	Ti(6)	Sb(5)	2.6971(18)
	Ti(9)	2.8527(12)		Sb(6)	2.7565(18)
	Ti(1)	3.0139(7)		Ti(8)	2.7986(24)
				Sb(7)	2.8925(16)
				Sb(6)	3.1427(8)
Sb(6)	Ti(7)	2.7549(12)	Ti(7)	Ti(7)	2.6594(23)
	Ti(6)	2.7565(18)		Sb(6)	2.7549(12)
	Ti(8)	2.7764(18)		Sb(1)	2.8127(12)
	Ti(1)	2.8728(17)		Sb(3)	2.8237(12)
	Ti(5)	2.9767(17)		Sb(5)	2.8394(12)
	Ti(8)	3.1134(8)		Sb(4)	2.8563(12)
	Ti(6)	3.1427(8)		Ti(7′)	2.9083(23)
Sb(7)	Sb(7)	2.7521(8)	Ti(8)	Sb(4)	2.7253(17)
	Ti(4)	2.8096(14)		Sb(6)	2.7763(18)
	Sb(7′)	2.8156(8)		Ti(6)	2.7986(24)
	Ti(3)	2.8622(14)		Sb(7)	2.8627(16)
	Ti(8)	2.8627(16)		Sb(6)	3.1134(8)
	Ti(6)	2.8925(16)	Ti(9)	Ti(9)	2.7614(23)
	Ti(5)	2.9445(14)		Ti(9′)	2.8063(23)
	Ti(1)	2.9699(15)		Sb(2)	2.8270(12)
	Ti(2)	2.9834(14)		Sb(4)	2.8395(12)
				Sb(5)	2.8527(12)
				Sb(3)	2.8563(12)
				Sb(1)	2.8740(12)
				Sb(2′)	2.8915(12)

Note. Distances are in ångstroms.

the primary component in the structure. If a large amount of antimony was present then the thermal parameters would be negative since the difference in neutron scattering lengths between Sb and Sn is approximately 10%. Attempts to refine the data with both Sb and Sn on the same sites suggested that some Sn was mixing with the Sb sites in the

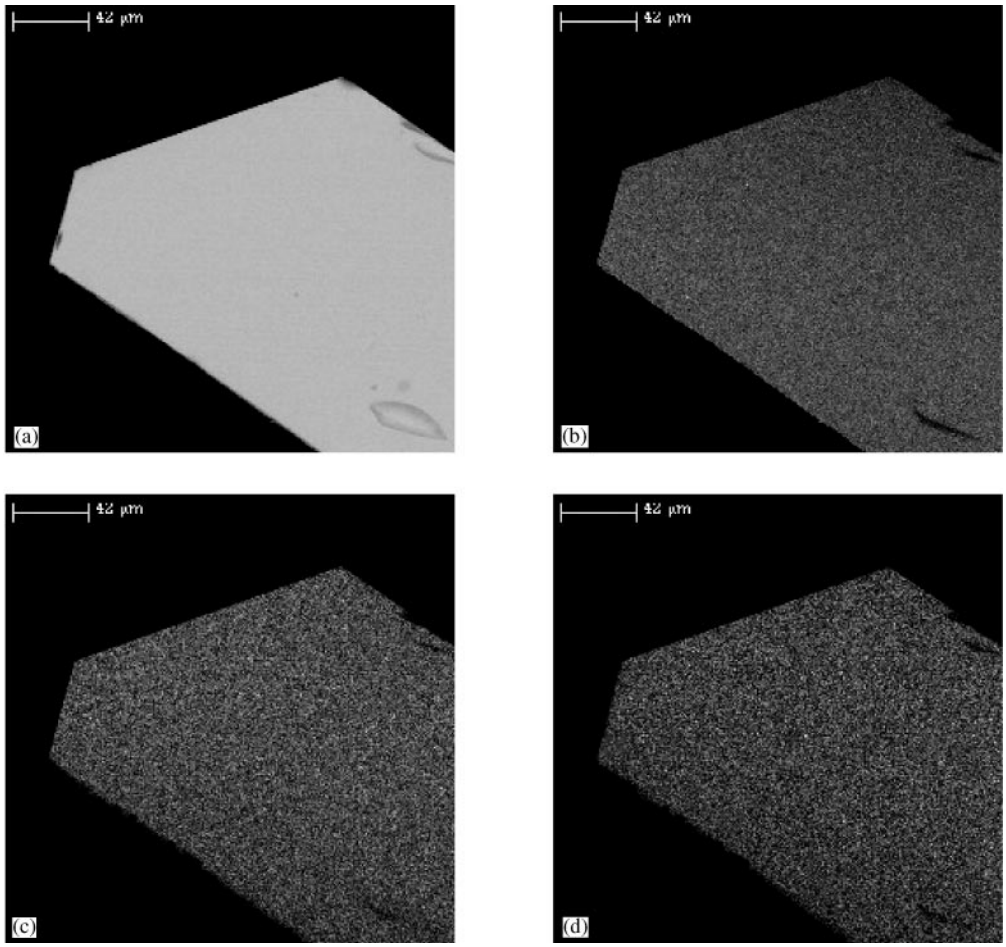

FIG. 1. (a) Backscattered electron image, (b) Ti X-ray dot map, (c) Sb X-ray dot map, and (d) Sn X-ray dot map of a $Ti_{11}(Sb,Sn)_8$ single crystal.

structure but large standard deviations in the Sb/Sn occupancies made this difficult to quantify. The final model only includes Ti and Sb. The refinements were performed with the GSAS program (21).

Elemental analysis. The composition of the title compound was examined with a Cameca SX-50 WDS microprobe operating at 20 keV accelerating potential and 10 nÅ beam current. Several single crystals were mounted in epoxy, which were then polished in order to provide analysis of the interior of the crystals. Ti metal, Sn metal, and $Eu_{14}MnSb_{11}$ (for Sb) were used as standards. A total of 60 spots (spot size: 1 μm) from six different areas of the three different crystals were analyzed and the net intensities of the peaks were converted to weight percentages using ZAF matrix corrections. The standard deviations of the analysis were between 0.16 and 0.76% from area to area. Figure 1 shows a back scattered electron image of the crystal along with the X-ray dot maps of Ti, Sb, and Sn atoms. This figure shows that there is a uniform distribution of both Sb and Sn atoms throughout the crystals.

Resistivity. Electrical resistivity measurement was performed on a crystal ($0.27 \times 0.28 \times 0.44\ cm^3$) using an in-line four-probe method from 15 to 300 K. Four Pt wires were attached to the sample using silver paint. The sample was placed on a homemade sample holder and transferred to a closed cycle refrigerator. A constant current (1 mÅ) was applied to the sample through the two outer leads (Keithley Model 224 current source) and the voltage was measured across the two inner leads (Keithley Model 196 nanovoltmeter). Electrical resistivity as a function of temperature was first measured parallel to the crystal axis, *b*. For the perpendicular measurement, the crystal was cut ($0.27 \times 0.28 \times 0.21\ cm^3$) and polished to minimize the influence of the crystal geometry.

Magnetism. Magnetic property measurements were made using a Quantum Design superconducting quantum interference device (SQUID) magnetometer with a 7-T superconducting magnet. The data were collected with the magnetic property measurement system (MPMS) software supplied by Quantum Design. A powder sample was placed

in a gel-capsule fixed in a straw. The temperature-dependent magnetization data were collected by first measuring zero-cooled (ZFC) magnetization in the field while warming from 5 to 300 K, then measuring magnetization while cooling back to 5 K with the field applied to obtain the field-cooled (FC) data.

RESULTS AND DISCUSSION

Synthesis. The composition of the title compound was initially refined from X-ray data to be $Ti_{11}Sb_8$. However, since the compound was prepared from a Sn flux, the composition was suspect. Various models were examined such as nonstoichiometry, site preference, and substitutional disorder in the X-ray diffraction data refinement; however, R_1 and wR_2 were not sensitive to the models employed. Microprobe showed a varying Sb and Sn concentration with the Sb/Sn ratio ranging from 0.98 to 1.40, depending on the samples. In order to investigate the Sb/Sn ratio further, the synthesis was explored more fully.

The reactions needed to produce two endmembers and an intermediate stoichiometry, $Ti_{11}Sb_{8-x}Sn_x$ ($x = 0$, 3.5, 8), were attempted by heating the corresponding elements in sealed Ta tubes enclosed in silica to 1100°C at a rate of 50°C/h, dwelling for 10 days, and furnace-cooling to room temperature. The powder diffraction pattern of the product ($x = 3.5$, Sb/Sn = 1.29) is in good agreement with that calculated from the single-crystal X-ray data for $Ti_{11}(Sb, Sn)_8$. There are no unindexed lines. In the case of the reaction to produce $Ti_{11}Sb_8$, diffraction peaks identified as the orthorhombic phase of $Ti_{10.84}Sb_{7.73}$ (7) were found to be present in the powder XRD along with unidentified peaks. In the case of the reaction to produce $Ti_{11}Sn_8$, there were no notable amounts of the phase corresponding to that calculated and unreacted Ti and Sn were found in the powder XRD.

The new As analog of the compound was also attempted in order to prepare $Ti_{11}As_{4.5}Sn_{3.5}$, in which Sb is substituted with the same group element, As, and mixed occupancies of As and Sn could be possibly determined by X-ray diffraction analysis due to their greater scattering factor difference. The stoichiometric mixture of the elements (Ti:As:Sn, 11:4.5:89) was placed in an alumina crucible and heated with the same temperature scheme used for the Sn-flux reaction of the title compound. The analysis of the X-ray powder diffraction pattern of the product confirms that the orthorhombic phase of the title compound was not obtained. A reaction of the elements (Ti:As:Sn, 11:4.5:3.5) in a sealed tantalum tube at 1100°C was also carried out and was unsuccessful in producing the orthorhombic phase.

Sb and Sn have approximately 10% neutron scattering length difference (coh b of Sb = 5.57 fm, coh b of Sn = 6.225 fm). If the two elements had any noticeable site preference, it should be distinguished by neutron diffraction. Neutron single-crystal diffraction was performed on a single crystal ($1.0 \times 1.0 \times 3.0$ mm^3). The refinement with all Sb provided $R_w(F^2) = 0.101$, whereas for all Sn, $R_w(F^2) = 0.104$. If occupancies for the all Sb-containing compounds were allowed to vary, they stayed fully occupied. From these combined experimental results (X-ray, neutron, synthesis), we propose that the exact site preference of Sb and Sn in this compound cannot be determined.

The $Ti_{11}(Sb,Sn)_8$ compound could be an example of a DFSO compound in that it has variable composition of Sb and Sn. Consistent with the DFSO definition, $Ti_{11}Sb_8$ can only be prepared with defects (7) and $Ti_{11}Sn_8$ is not known. The general DFSO concept (2) requires that the structure type of the endmembers of the compound be unknown and also requires that the fractional site occupancies are more or less fixed per site, and differ from one site to another. In the case of $Ti_{11}(Sb, Sn)_8$, it is clear that the structure type is unknown in the binary systems and the structure requires both Sb and Sn in the anion sites; however, the site preference cannot be determined. If this is truly a DFSO compound, it may be only be verified by substitution of Ge/Pb on the various sites of Sn.

Structure. For the purpose of discussion, the structure of $Ti_{11}(Sb,Sn)_8$ will be described here after as $Ti_{11}Sb_8$. The structure of the $Ti_{11}Sb_8$ compound can be described as containing two repeating layers that are S_2 symmetric to each other with interstitial atoms that are closely connected to make linear chains. Figure 2a shows four layers with the interpenetrating, perpendicular linear chains. Figure 2b shows the channel-like structure that can be derived from the repeating layers with Ti or Sb linear chains running through the center of the channels. Seven crystallographically unique Ti sites and six different Sb sites are embedded in a layer, making a planar network of mixed Ti and Sb, and the two remaining Ti sites (Ti(7), Ti(9)) and one Sb site (Sb(7)) are positioned between these layers making the linear chains. In all, a total of nine crystallographically unique Ti atoms and seven different Sb atoms occur with high coordination numbers. This is typical for such intermetallic compounds.

This structure type has been described in relation to the classical W_5Si_3 structure (22). Figure 3 shows a perspective view down the c axis of the W_5Si_3 structure. When this structure is compared to Fig. 2b, the structural similarities are apparent. The common four polyhedral stacks, containing two metal linear chains (Ti or W) and two anion linear chains (Sb or Si), which are the main repeating units in both structures, can be found in both figures.

In Fig. 4, differences between the two types of polyhedra of $Ti_{11}(Sb, Sn)_8$ and W_5Si_3 are compared. In the $Ti_{11}(Sb, Sn)_8$ compound, six Ti atoms and six Sb atoms are coordinated to the central Ti atom with distances at 3.188–3.349 Å and 2.755–2.856 Å, respectively, in the Ti–Sb

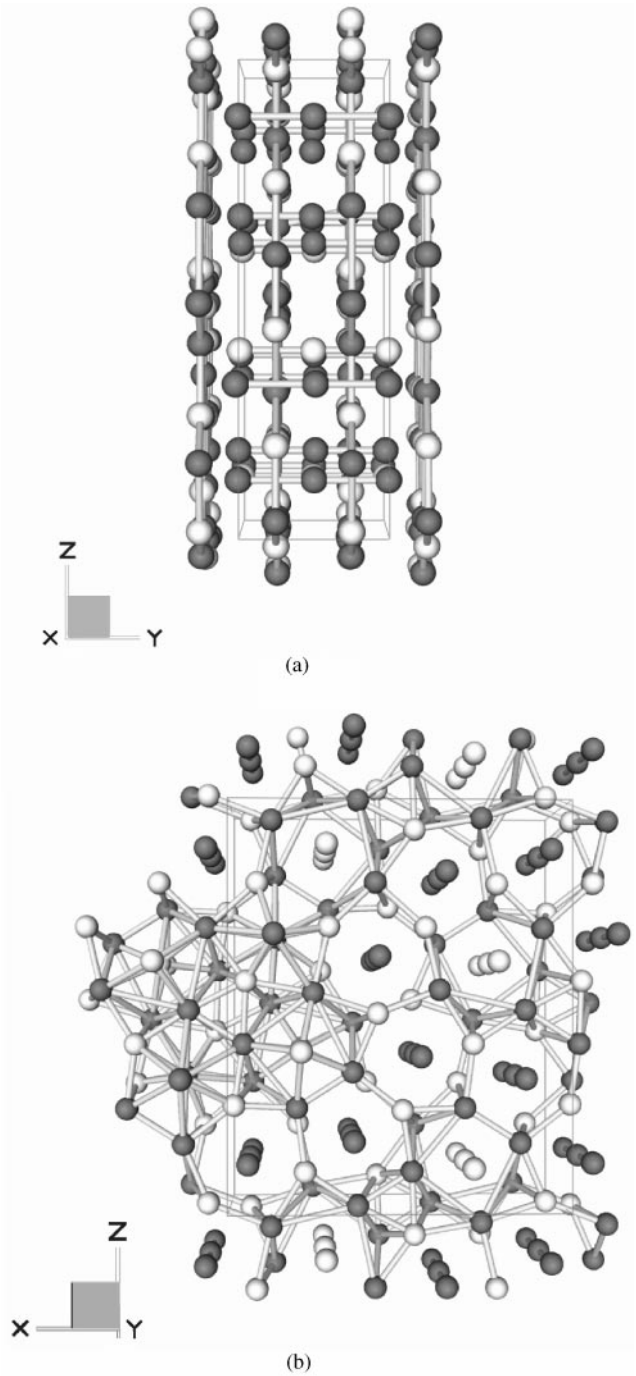

FIG. 2. (a) Perspective view down the *a* axis and (b) perspective view down to the *b* axis of the structure of $Ti_{11}(Sb, Sn)_8$. Gray circles, Ti; white, Sb.

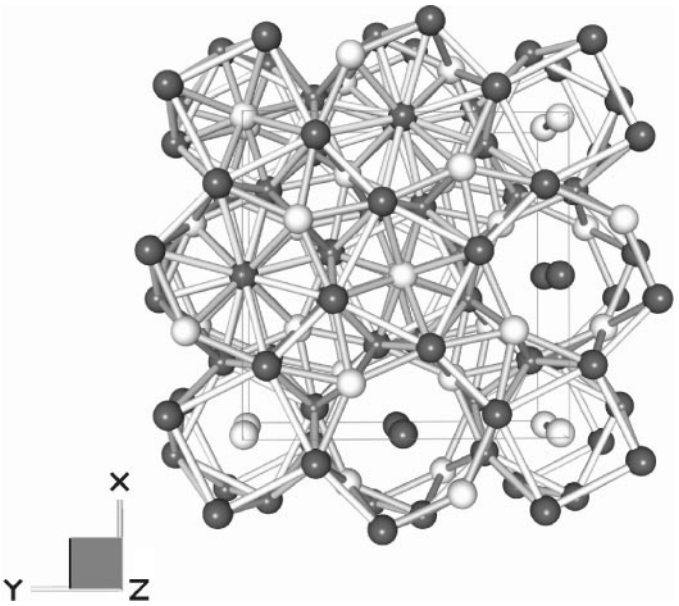

FIG. 3. Perspective view down to *c* axis of the W_5Si_3 structure. Gray circles, W; white, Si.

polyhedra (Fig. 4a), and seven Ti atoms are coordinated to the central Sb atom with distances at 2.810–2.983 Å in the Ti polyhedra (Fig. 4b). In the Ti polyhedra, one Ti is missing compared to the ideal W_5Si_3-type structure (Fig. 4d). In the W_5Si_3 structure, eight W atoms and four Si atoms are coordinated to the central W atom with same distances in the W–Si polyhedra (Fig. 4c) and eight W atoms are coordinated to the central Si atom with a same distance in the W polyhedra (Fig. 4d). These central W and Si atoms are connected to each other to make linear chains. In the case of the W polyhedra, they stack along the same direction as the linear chain to make the characteristic square antiprism–prism column that is an important building block sequence in the $A_{5n+6}B_{3n+5}$ family (23–25). In addition, $Ti_{11}(Sb, Sn)_8$ contains a metal M_{10} polyhedron (a Sb is surrounded by 10 Ti) that is observed with all members of the $A_{5n+6}B_{3n+5}$ family, shown in Fig. 5. The antiprism–prism columns are laterally separated by these common anion-centered M_{10} polyhedra (25).

The interatomic distances in the compound may be properly reviewed on the basis of the previously discussed main building blocks of the layers and linear chains. The relatively large Ti–Ti distances ranging from 3.077 to 3.577 Å, longer than that in *hcc* Ti (2.94 Å) (26), were found in the interstitial atoms and interlayer. In the linear units and intralayer, the Ti–Ti distances range from 2.659 to 2.909 Å, indicating strong interactions. The same trend was observed in Sb–Sb distances. The alternating Sb–Sb bonds of 2.752 and 2.816 Å, shorter than that in elemental antimony (2.91 Å, α-rhombohedral) (27), were found in the linear chains and the other longer distances, ranging from 3.327 to 3.363 Å, occur between layers with negligible interactions. The Ti–Sb distances have a relatively uniform distribution, ranging from 2.722 to 2.976 Å (intralayer), from 2.755 to 2.983 Å (within polyhedral stacks), and from 2.940 to 3.143 Å (interlayer).

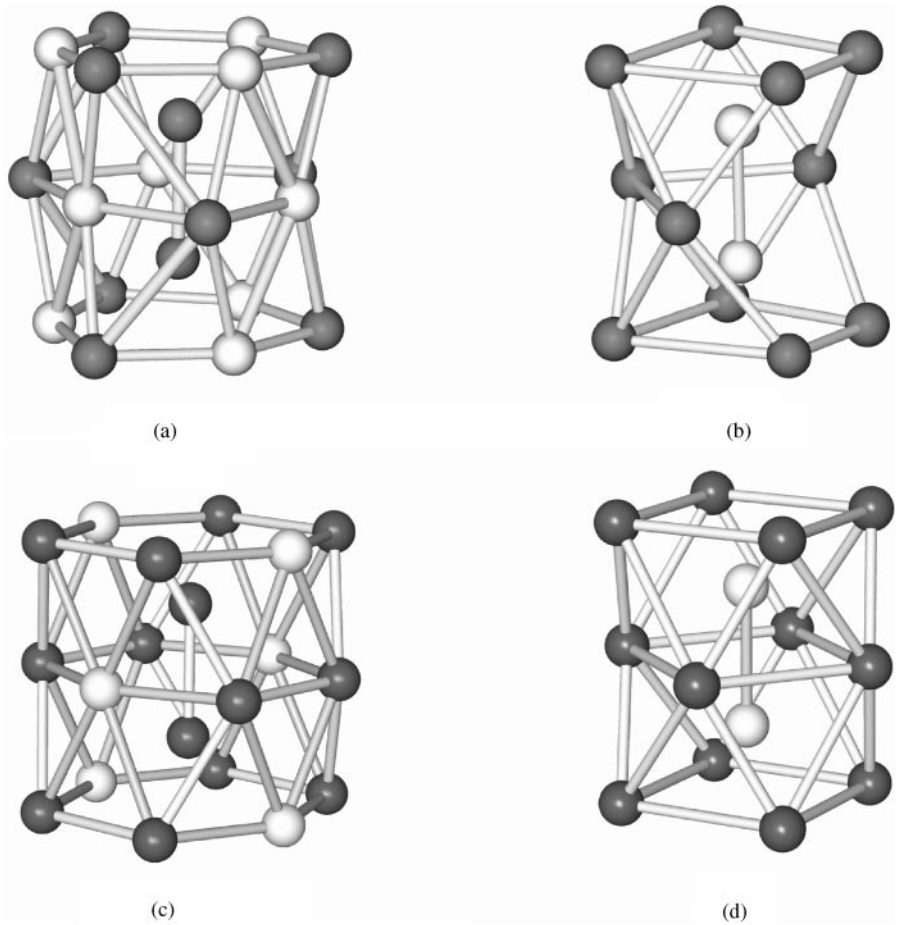

FIG. 4. (a) Ti–Sb polyhedra about a linear Ti chain, (b) Ti polyhedra about a linear Sb chain in $Ti_{11}(Sb,Sn)_8$, gray circles, Ti; white, Sb, and (c) W–Si polyhedra about a linear W chain, (d) W polyhedra about a linear Si chain, gray circles, W; white, Si.

Figure 6 shows the plot of electrical resistivity as a function of temperature and confirms that the $Ti_{11}(Sb, Sn)_8$ compound is metallic. The resistivity, which was measured

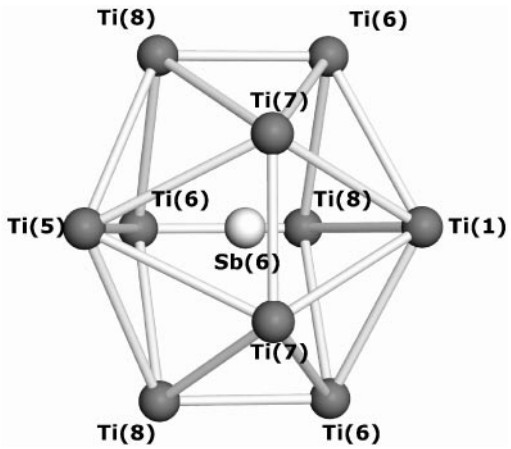

FIG. 5. The characteristic M_{10} polyhedra (a Sb is surrounded by 10 Ti) in the $A_{5n+6}B_{3n+5}$-type structure.

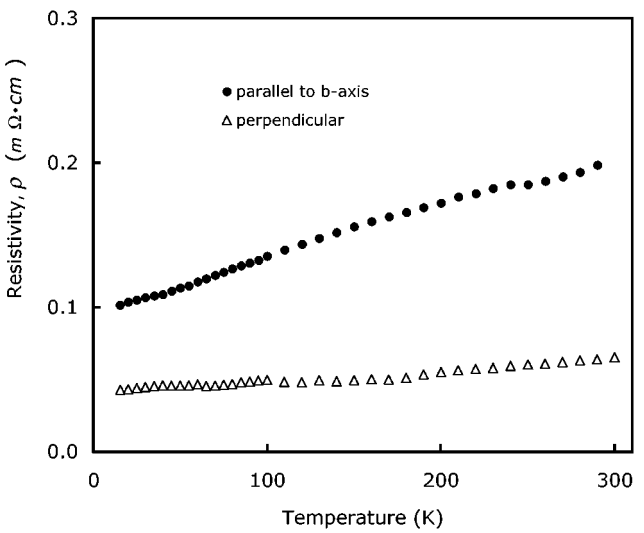

FIG. 6. Resistivity vs temperature from 15 to 300 K for a $Ti_{11}(Sb, Sn)_8$ single crystal.

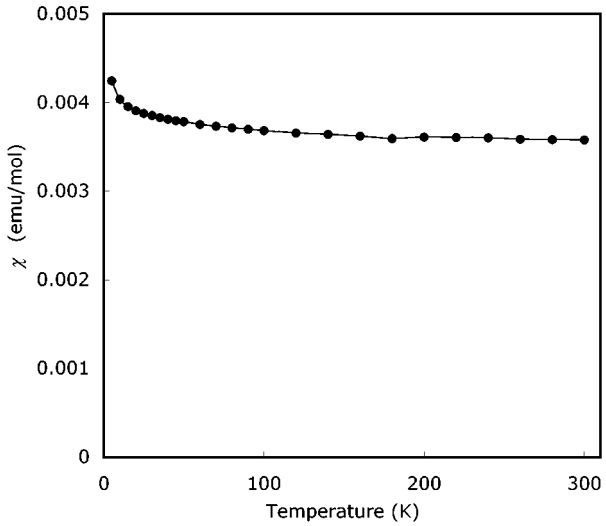

FIG. 7. Temperature-dependent magnetization of a powder sample of $Ti_{11}(Sb,Sn)_8$.

parallel to the crystal axis *b*, decreases from 2.0×10^{-1} m$\Omega \cdot$cm to 1.0×10^{-1} m$\Omega \cdot$cm as temperature decreases from 300 to 15 K and its ratio is $\rho_{300}/\rho_{15} \approx 2$. In contrast, the perpendicular resistivity, resistivity along the *a* or *c* axis, ranges from 0.65 to 0.43×10^{-1} m$\Omega \cdot$cm in the same temperature range and shows slightly less temperature dependence ($\rho_{300}/\rho T_{15} \approx 1.5$). This anisotropic electrical resistivity is consistent with the description of the crystal structure. The electrical transport along the *a* or *c* axis, i.e., intralayer, experiences less resistance than the transport across layers. The electronic structure of $(Zr,V)_{11}Sb_8$ was determined (8) and showed a high density of states at the Fermi level, being composed primarily of metal orbitals. Magnetization as a function of temperature is shown in Fig. 7 and provides good agreement with the resistivity measurement, showing very weak temperature dependence of magnetic susceptibility above 80 K ($\chi_{300}/\chi_{80} = 0.96$). The data are the same regardless of how the sample is measured (ZFC, FC) and therefore only ZFC data are shown. This behavior is similar to the free-electron Pauli paramagnetic susceptibility (28) occurring in metals and is attributed to the high density of *d* states of Ti atoms at the Fermi level, which forms the conduction band.

ACKNOWLEDGMENTS

We thank R. N. Shelton for use of the magnetometer, P. Klavins for useful discussions, and the X-ray analytical lab housed in the Geology Department, UC Davis, for microprobe analysis. The research was funded by National Science Foundation (DMR-9803074). This work has benefited from the use of the Intense Pulsed Neutron Source at Argonne National Laboratory funded by the U.S. Department of Energy, BES-Material Science under Contract W-31-109-Eng-38.

REFERENCES

1. G. J. Miller, *Eur. J. Inorg. Chem.* **5,** 523 (1998).
2. H. F. Franzen and M. Köckerling, *Prog, Solid State Chem.* **23,** 265 (1995).
3. R. S. Mulliken, *J. Chem. Phys.* **23,** 1841 (1995).
4. K. W. Richter and H. F. Franzen, *J. Solid State Chem.* **150,** 347 (2000).
5. H. Kleinke and H. F. Franzen, *J. Am. Chem. Soc.* **119,** 12824 (1997).
6. X. Yao and H. F. Franzen, *J. Solid State Chem.* **86,** 88 (1990).
7. H. Kleinke, *Z. Kristallogr. Supplem.* **16,** 42 (1999).
8. H. Kleinke, *J. Mater. Chem.* **9,** 2703 (1999).
9. P. Israiloff, H. Völlenke, and A. Wittmann, *Monatsh. Chem.* **105,** 1387 (1974).
10. O. G. Karpinskii and A. V. Arakcheeva, *Izv. Akad. Nauk SSSR, Met. IZNMA* **5,** 196 (1984).
11. P. C. Canfield and Z. Fisk, *Phil. Mag. B* **65,** 1117 (1992).
12. S. M. Kauzlarich (Ed.), "Chemistry, Structure, and Bonding of Zintl Phases and Ions," p. 245. VCH, New York, 1996.
13. CrystalDiffract, Version 2.0: CrystalMaker Software, Oxfordshire, UK, 1997.
14. SMART: Siemens Analytical X-ray Systems, Inc., Madison, WI, 1994.
15. SAINT, Version 6: Siemens Analytical X-ray Systems, Inc., Madison, WI, 1999.
16. G. M. Sheldrick, *SHELXTL Version* 5.10, Bruker AXS Inc., Madison, WI, 1997.
17. R. Lam and A. Mar, *Inorg. Chem.* **35,** 6959 (1996).
18. A. J. Schultz, K. Srinivasan, R. G. Teller, J. M. Williams, and C. M. Lukehart, *J. Am. Chem. Soc.* **106,** 999 (1984).
19. R. A. Jacobson, *J. Appl. Cryst.* **19,** 283 (1986).
20. J. A. K. Howard, O. Johnson, A. J. Schultz, and A. M. Stringer, *J. Appl. Cryst.* **20,** 120 (1987).
21. A. C. Larson and R. B. Von Dreele, "GSAS—General Structure Analysis System." Los Alamos National Laboratory, 1994.
22. Aronsson, *Acta Chem. Scand.* **9,** 1107 (1955).
23. E. Parthé and J. T. Norton, *Acta Crystallogr.* **11,** 14 (1958).
24. J. Le Roy, J. M. Moreau, and D. Paccard, *J. Less-Comm. Met.* **76,** 131 (1980).
25. E. A. Leon-Escamilla, W. Hurng, E. S. Peterson, and J. D. Corbett, *Inorg. Chem.* **36,** 703 (1997).
26. N. N. Greenwood and A. Earnshaw, "Chemistry of the Elements," 2nd ed., p. 957. Butterworth-Heinemann, Oxford, 1997.
27. N. N. Greenwood and A. Earnshaw, "Chemistry of the Elements," 2nd ed., p. 551. Butterworth-Heinemann, Oxford, 1997.
28. H. P. Myers, "Introductory Solid State Physics," 2nd ed., p. 232. Taylor & Francis, London, 1997.